

Tuning band gaps in twisted bilayer MoS₂

Yipei Zhang,¹ Zhen Zhan,^{1,*} Francisco Guinea,^{2,3} Jose Ángel Silva-Guillén,¹ and Shengjun Yuan^{1,†}

¹*Key Laboratory of Artificial Micro- and Nano-structures of Ministry of Education and School of Physics and Technology, Wuhan University, Wuhan 430072, China*

²*Fundación IMDEA Nanociencia, C/Faraday 9, Campus Cantoblanco, 28049 Madrid, Spain*

³*Donostia International Physics Center (DIPC)UPV/EHU, E-20018 San Sebastián, Spain*

In the emerging world of twisted bilayer structures, the possible configurations are limitless, which enables for a rich landscape of electronic properties. In this paper, we focus on twisted bilayer transition metal dichalcogenides (TMDCs) and study its properties by means of an accurate *ab initio* tight-binding model. We build structures with different angles and find that the so-called flatbands emerge when the twist angle is sufficiently small (around 7.3°). Interestingly, the band gap can be tuned up to a 5% (104 meV) when the twist angle varies from 21.8° to 0.8°. Furthermore, when looking at local density of states we find that the band gap varies locally along the moiré pattern due to the change in the coupling between layers at different sites. Finally, we also find that the system can suffer a transition from a semiconductor to a metal when a sufficiently strong electric field is applied. Our study can serve as a guide for the practical engineering of the TMDCs optoelectronic devices.

1. INTRODUCTION

Although graphene has been known for some time now¹, recently there has been a renewed interest in the properties of bilayer structures due to the discovery of strongly correlated effects in these structures at certain small (magic) twist angles.² This finding triggered a handful of experimental and theoretical studies in that kind of structures where not only strongly correlated effects such as superconductivity and quantum phase transitions^{3–13}, but also the existence of pseudo-magnetic fields due to the strain that the system can experience either by applying externally a mechanical strain^{14,15} or due to intrinsic strain that appears in the moiré pattern because of the incommensurability of the superstructures.¹⁶

Similarly to graphene, group V-B transition metal dichalcogenides (from now on TMDCs), are exfoliated materials that have an hexagonal structure and also change their electronic properties dramatically when lowering the number of layers to one. Interestingly, in contrast to graphene, TMDCs are semiconducting and, moreover, the nature of this band gap depends on the number of layers changing from indirect to direct when the system goes from multi-layer to monolayer.¹⁷ The fact that monolayer TMDCs present a direct band gap overcomes one of the major drawbacks of graphene for its integration to modern electronic and optoelectronic devices. Furthermore, this band gap can be tuned by means of the so-called straintronics¹⁸ methods or electric fields. Therefore, it seems like a natural and interesting step to study the electronic properties of twisted bilayer TMDCs. Recently, a theoretical work using density functional theory (DFT) methods predicted the existence of flatbands in MoS₂ when the twist angle is sufficiently small.¹⁹ Furthermore, an experimental work was carried out on another twisted bilayer TMDCs, WSe₂, where they found such flatbands when achieving small twist angles.²⁰ Interestingly, it has been shown that the different environment

surrounding the atoms due to the change in the stacking along the moiré pattern in heterobilayer TMDCs (a structure formed by a different TMDCs in each layer) entails a difference in the interlayer coupling, which results in a local change of the gap.²¹ Nevertheless, a thorough study of the electronic properties and their possible tunability of this kind of structures is still lacking.

In this work, we study the electronic properties of twisted bilayer MoS₂ and the possibility of tuning the band gap. The paper is organized in the following way: We first show how to build the commensurate twisted bilayer TMDCs and the method used to compute their electronic properties. Then, we study the tunability of these properties by means of a change in the rotation angle, by the variation of the local interlayer couplings due to the different stackings in the moiré pattern or by applying an electric field to the system.

2. THE COMMENSURATE BILAYERS

We consider bilayer TMDCs, which are composed of two monolayers of MoS₂ rotated in the plane by an angle θ . Since the two layers have the same lattice constant, following the same method as in twisted bilayer graphene, the moiré supercell can be constructed by identifying a common periodicity between the two layers²². We start from the 2H stacking of MoS₂, that is with the Mo (S) atom in the top layer directly above the S (Mo) in the bottom layer, and choose the rotation origin, O, at an atom site. For one layer, we define a supercell with a basis vector $\mathbf{V}_1 = n\mathbf{a}_1 + m\mathbf{a}_2$, being \mathbf{a}_1 and \mathbf{a}_2 the lattice vectors of single-layer MoS₂, and n and m are non-negative integers with $n - m = 1$, which means that the supercell contains only one moiré pattern. For the second layer, a cell with the same size and rotated by an angle θ can be obtained with the basis vector $\mathbf{V}_2 = (n + m)\mathbf{a}_1 - m\mathbf{a}_2$. Then, the commensurate bilayers with the twist angle θ can be achieved by rotating the cell with \mathbf{V}_1 by $\theta/2$ and

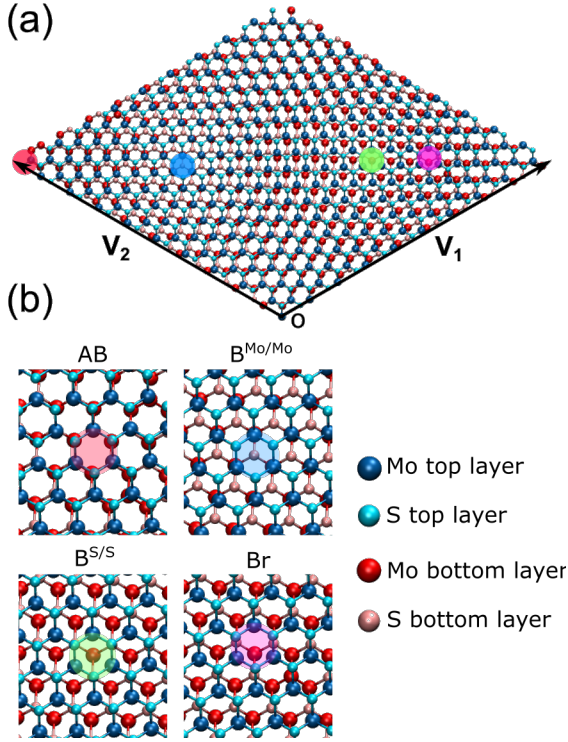


FIG. 1: (a) The moiré superlattice of twist bilayer MoS₂ with rotation angle $\theta = 3.5^\circ$. (b) Zoom in around the atomic structures of different high symmetry points. The AB, B^{Mo/Mo}, B^{S/S} and Br regions are highlighted by circles of different colors.

rotating the cell with \mathbf{V}_2 by $-\theta/2$. The rotation angle is given by:

$$\cos \theta = \frac{n^2 + 4nm + m^2}{2(n^2 + nm + m^2)} \quad (1)$$

The commensurate supercell contains $N = 6(n^2 + nm + m^2)$ atoms, and the lattice constant can be simplified as $|\mathbf{V}_1| = |\mathbf{V}_2| = \frac{a}{2\sin(\theta/2)}$, where $a = 3.16 \text{ \AA}$ is the lattice constant of the single-layer MoS₂²³. Fig. 1(a) shows a twisted bilayer MoS₂ structure with the twist angle $\theta = 3.5^\circ$, which is obtained with $n = 10$ and $m = 9$. The moiré superlattice contains 1626 atoms. In a supercell with relatively small twist angle there are several high-symmetry stacking patterns, for instance, AB, B^{Mo/Mo} and B^{S/S}. In the AB stacking, the Mo atoms of layer 1 are over the S atoms of layer 2 and the S atoms of layer 1 are over the Mo atoms of layer 2. For B^{Mo/Mo}, Mo of layer 1 are over Mo of layer 2 and all S of one layer are located in the center of hexagons of the other layer. For B^{S/S}, S of layer 1 are over S of layer 2 and all Mo of one layer are in the center of hexagons of the other layer. The Br site is located at one third of the B^{S/S} – AB path. All of these special sites are illustrated in Fig. 1(b).

3. NUMERICAL METHOD

By using the first-principles density function theory (DFT), ultraflatbands at the valence band edge are discovered in twisted bilayer MoS₂^{19,24}. Up to now, the largest system of this kind calculation using first-principles methods contains 4902 atoms, which corresponds to a twist angle of 2.0° . Although it is possible to perform calculations on larger systems, there are some limitations due to the computational resources when the twist angle becomes smaller since the number of atoms increases sharply. This larger structures can be more easily systematically studied by utilizing a tight-binding method. For instance, the system with the electronic properties calculated by diagonalization in reciprocal space contains up to 59644 orbitals, which corresponds to $\theta = 1^\circ$. In this paper, we will use another approach, tight-binding propagation method (TBPM), which is based on the numerical solution of the time-dependent Schrödinger equation without any diagonalization²⁵. The TBPM can tackle systems with the number of orbitals as large as ten million, for instance, the extremely tiny twist angle in twisted bilayer graphene¹⁶ and bilayer graphene quasicrystal²⁶. More importantly, defects, magnetic and electric fields can be easily implemented in this approach.

In order to calculate the electronic band structures of twisted bilayer TMDCs, we use an accurate tight-binding Hamiltonian introduced in Ref. 27. The minimum atomic orbital basis to correctly describe TMDCs are the five *d* orbitals of the transition-metal atom and three *p* orbitals of the two chalcogen atoms.^{28,29} This model well reproduces the band structure calculated by *ab-initio* DFT method with *GW* quasi-particle correction in the low energy region. For bilayer TMDCs, the total Hamiltonian can be written as^{27,30}:

$$\hat{H} = \hat{H}_1^{(1L)} + \hat{H}_2^{(1L)} + \hat{H}_{int}^{(2L)}, \quad (2)$$

where $\hat{H}_{1(2)}^{(1L)}$ is the eleven-orbital single layer Hamiltonian and $\hat{H}_{int}^{(2L)}$ is the interlayer Hamiltonian. The $\hat{H}_{1(2)}^{(1L)}$ contains the on-site energy, the hopping terms between orbitals of the same type at first-neighbor positions and the hopping terms between orbitals of different type at first- and second-neighbor positions. The interlayer hopping Hamiltonian only includes the interaction between the chalcogen atoms at the interface of the bilayer:

$$\hat{H}_{int}^{2L} = \sum_{p'_i, \mathbf{r}_2, p_j, \mathbf{r}_1} \hat{\phi}_{2, p'_i}^\dagger(\mathbf{r}_2) t_{p'_i, p_j}^{(LL)}(\mathbf{r}_2 - \mathbf{r}_1) \hat{\phi}_{1, p_j}(\mathbf{r}_1) + h.c. \quad (3)$$

where $\hat{\phi}_{i, p_j}$ is the p_j orbital basis of i -th monolayer. Within the Slater-Koster approximation, the hopping terms can be expressed as:

$$t_{p'_i, p_j}^{(LL)}(\mathbf{r}) = (V_{pp, \sigma}(r) - V_{pp, \pi}(r)) \frac{r_i r_j}{r^2} + V_{pp, \pi}(r) \delta_{i, j}, \quad (4)$$

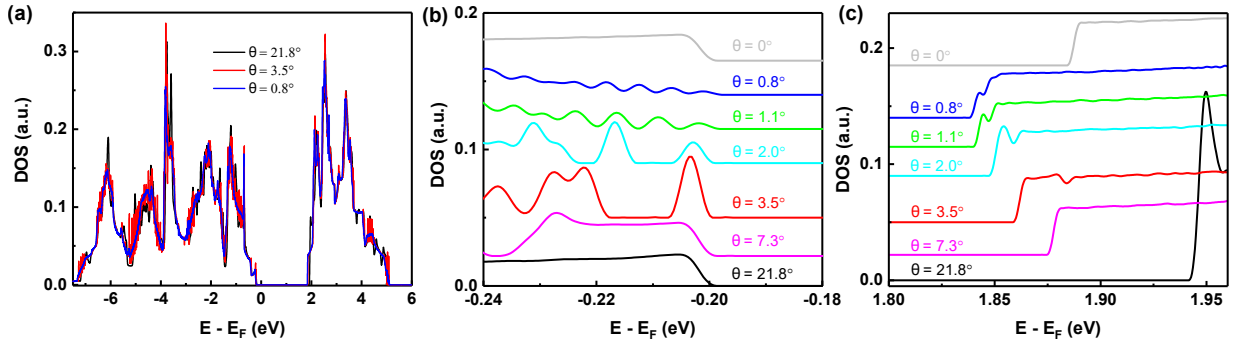


FIG. 2: (a) The calculated DOS of twisted bilayer MoS₂ bilayers with different twist angles. (b) and (c) The detailed changes of DOS near the valence and conduction band extrema, respectively.

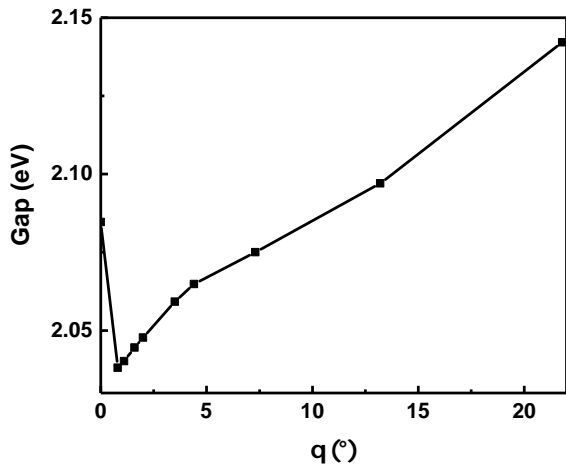


FIG. 3: The band gap E_g between the CBM and VBM of twisted bilayer MoS₂ with different rotation angles.

where $r = |\mathbf{r}|$ and the distance-dependent Slater-Koster parameter is:

$$V_{pp,b} = \nu_b e^{[-(r/R_b)^{\eta_b}]}, \quad (5)$$

where $b = \sigma, \pi$, ν_b , R_b and η_b are constant values that are dependent on the specific of the chalcogen interlayer interactions, of which values are taken from the Ref. 27. In our calculations, only the interlayer hopping terms between a pair of chalcogen atoms that are separated by a distance less than 8 Å are included.

In all the calculations, we use a large enough system with more than 10 million orbitals to ensure the convergence of the results. Periodic boundary conditions are used in the simulation. For the density of states (DOS) and local density of states (LDOS), the number of time integration steps determines the energy resolution in the TBPM method. In all the calculations the time steps are set to 4096, which gives an energy resolution of 1.8 meV. Furthermore, we can use the TBPM to obtain the map of the amplitudes of the quasieigenstates which has been shown to be in agreement with the measured dI/dV mapping in Ref. 16.

4. RESULTS AND DISCUSSION

4.1. Tuning the band gap by rotation angle

It has been proved that the twist angle has a significant influence on the electronic properties of twisted bilayer TMDCs^{31–35}. All these studies are mainly focused on large rotation angles. Interestingly, ultraflatbands are detected in low-angle twisted bilayer MoS₂, which provide a platform for exploring new physical phenomena, for instance, the Mott-insulating phase at half-filling of the band^{2,19}. This leaves important questions unaddressed: Are there ultraflatbands in twisted TMDCs with tiny twist angle? What exotic features will be found in low-angle twisted bilayer TMDCs?

In this part, we study the density of states of twisted bilayer MoS₂ with various rotation angles. The smallest rotation angle that we calculate is 0.8° deg which results in a Moré pattern that contains 29526 atoms (108262 orbitals), which is far beyond the ability of state-of-the-art first-principles methods and tight-binding methods where the electronic structure is calculated using diagonalization methods. The DOS of twisted bilayer MoS₂ with an angle from 0° to 21.8° are plotted in Fig.2 (a). It is clear that the DOS varies significantly depending on the angle, especially for the DOS deep into the valence band, which is in good agreement with the calculated results in Ref. 36. More interesting things happen near the band edges. In order to investigate this, the detailed evolution of DOS near the band edge is illustrated in Fig.2 (b) and (c). We see clearly that, as the twist angle decreases, the valence band edge energy increases while the conduction band edge energy decreases. Thus the energy gap decreases as the twist angle decreases. That is, the band gap can be engineered through the control of the rotation angle. As shown in Fig. 3, the band gap reduces by 104 meV (around 5% change) when changing the rotation angle from 21.8° to 0.8°. Note that, for samples with small twist angle, some energy peaks appearing near the valence band edges correspond to the detected ultraflatbands. For instance, in the DOS of the twisted bilayer MoS₂ with twist angle $\theta = 3.5$, the peak located

at -0.2 eV corresponds to the ultraflatband discovered in Ref. 19,37. Furthermore, there is an angle from which the flatband emerges. This is consistent with reported experimental and DFT results.^{19,20}

4.2. Tuning the band gap by interlayer coupling at different high-symmetry stacking points

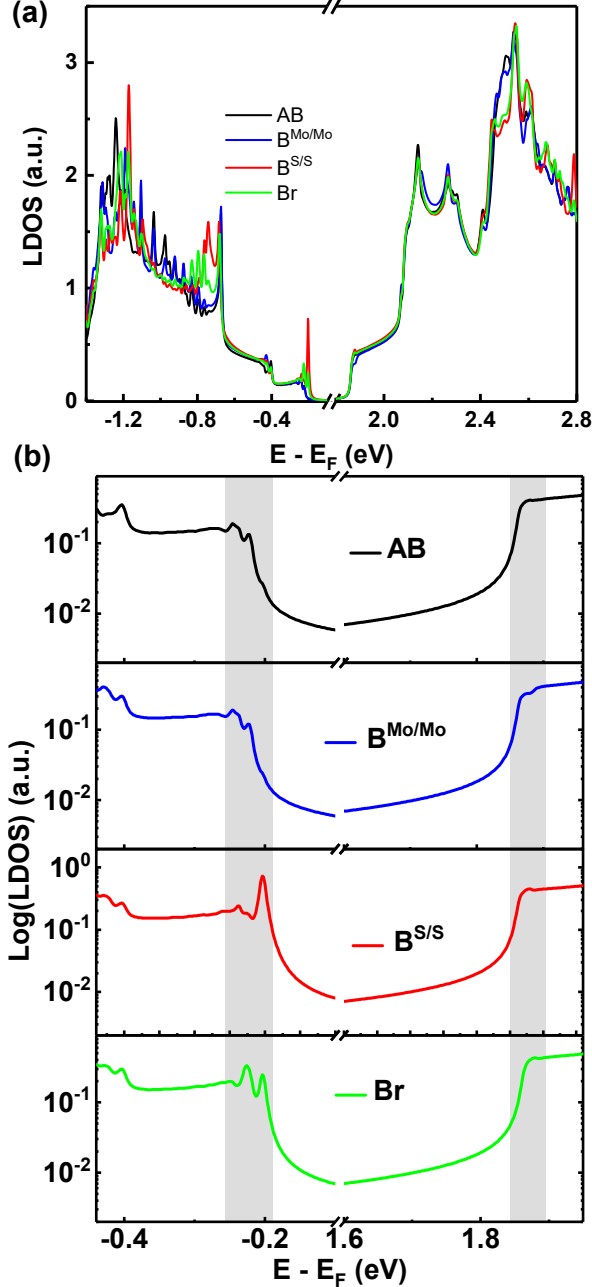


FIG. 4: (a) The calculated LDOS of the AB, $B^{Mo/Mo}$, $B^{S/S}$ and Br regions in twisted bilayer MoS_2 sample with $\theta = 3.5^\circ$. The inset is the zoom-in of the LDOS near the valence and conduction band edges. (b) The logarithmic scales of the LDOS near the valence and conduction band edges.

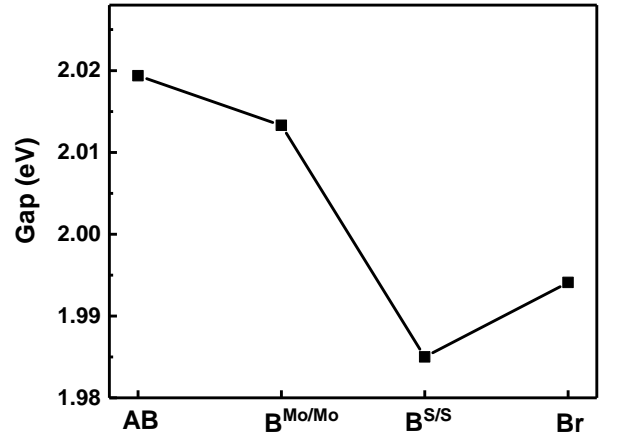


FIG. 5: The local band gap E_g of the AB, $B^{Mo/Mo}$, $B^{S/S}$ and Br regions in twisted bilayer MoS_2 with $\theta = 3.5^\circ$.

It has been shown that, for heterostructures composed of monolayers of two different TMDCs, the local band gap is periodically modulated by the interlayer coupling at different high-symmetry points with an amplitude of ~ 0.15 eV²¹. Can the interlayer coupling be used as a parameter to tune the local band gap for the twisted homobilayer TMDCs (the heterostructure composed of the same monolayers TMDCs)? To answer this question, we calculate the local density of states for the twisted bilayer MoS_2 with $\theta = 3.5^\circ$ at the high symmetry stacking points AB, $B^{Mo/Mo}$, $B^{S/S}$ and Br (illustrated in Fig.1).

The results are shown in Fig.4(a). Similar to the DOS in Fig. 2, the interlayer coupling changes also significantly the LDOS deep into the valence band. The details of the LDOS near the valence band maximum (VBM) and conduction band minimum (CBM) are plotted in Fig. 4(b). In the conduction band, the LDOS near the band edge are similar for the four high-symmetry sites. On the contrary, the VBM has a remarkable change due to the different interlayer coupling at the four points, which can be seen more clearly in the logarithm of the LDOS illustrated in Fig. 4(b). Furthermore, we find in Fig.4 that the ultraflatband signature, which corresponds to the peak with energy ~ -0.2 eV, only appears at $B^{S/S}$ and Br points. We can also see that the sharpest peak appears in $B^{S/S}$ sites. This is expected since at this position the top layer S atom sits directly above a bottom layer S atom, which gives the strongest interlayer interaction, given the fact that in our tight-binding model, interlayer coupling originates from hopping between S atoms in different layers. The absence of signals of flatband on other areas indicates that the localization of the electronic states of the flatband is around the $B^{S/S}$ site, which is in accordance with the localization of the VBM wave function in the rigidly twisted sample in Ref. 19. The local energy gap at different stacking regions is shown in Fig. 5. We can see how the band gap changes locally depending on the specific site. At $B^{S/S}$, which has the strongest interlayer coupling, we find the mini-

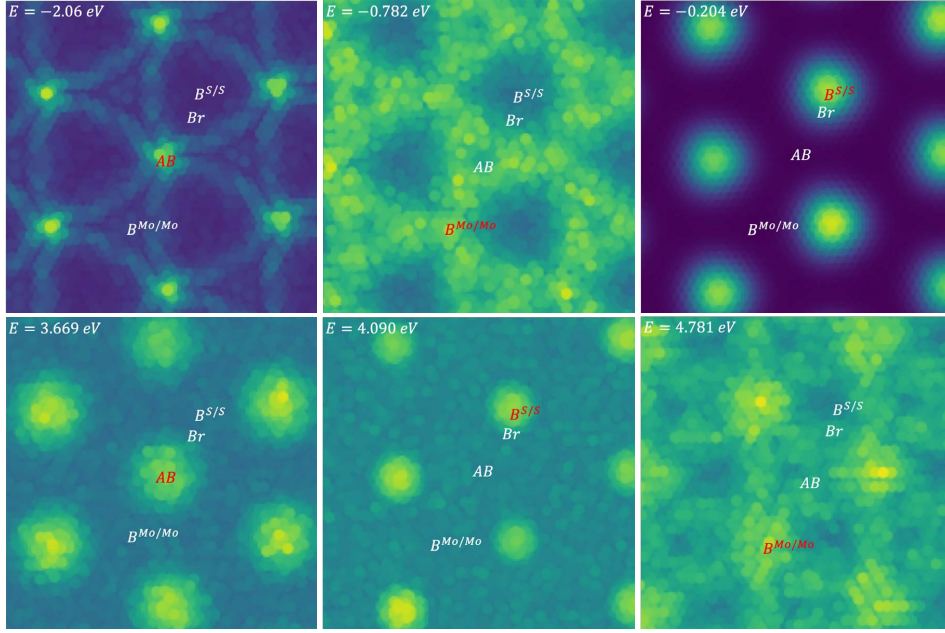


FIG. 6: Calculated LDOS mapping with different energies of the twisted bilayer MoS₂ with $\theta = 3.5^\circ$. The corresponding energies and the four special sites AB, B^{Mo/Mo}, B^{S/S} and Br are labeled in each image.

mum local energy gap. The local band gap is modulated periodically with an amplitude of ~ 35 meV. The evolution of such site-dependent local band gap is in agreement with the experimental results reported in heterostructure TMDCs²¹. All in all, an important consequence of the interlayer coupling in the Morié supercell is the tuning the local band gap at different stacking points.

The periodic variation of the local electronic structure as a consequence of different interlayer couplings is also visualized more clearly looking at the energy dependence of the spatial distribution of LDOS plotted in Fig. 6. For instance, at a high negative energy of -2.06 eV, where a peak appears in the LDOS of the AA site, the spectra at that same position is higher than that of the other three high-symmetry points. However, at -0.204 eV, where the spectral feature of the AA site is out of the tunneling range, the intensity of the AA site changes from a bright feature to a deep hole, whereas the B^{S/S} site has the highest spectral. As we discuss previously, all the states are localized at the B^{S/S} site at -0.204 eV. The continuous evolution of the local electronic spectral at different sites by different energies also occurs for positive energies. All these results show a periodic charge density modulation at different energies over large areas, which can be detected experimentally using scanning tunneling microscopy dI/dV mapping.

4.3. Tuning the band gap by applying an electric field

As it has been shown, a vertical electric field can open a bandgap in bilayer graphene^{38,39}. Furthermore, bilayer

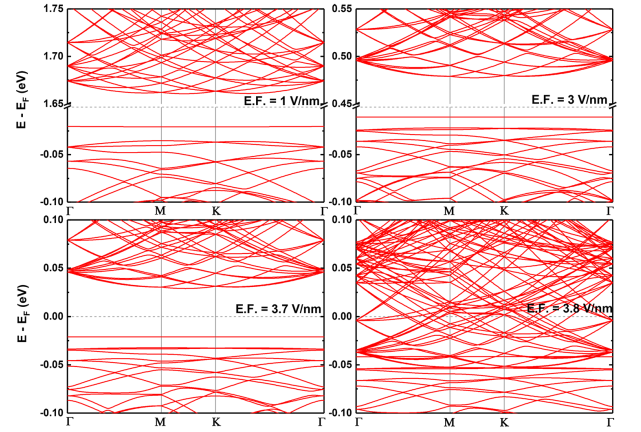


FIG. 7: Band structure of twisted bilayer MoS₂ with $\theta = 3.5^\circ$ along Γ - K - M - Γ direction in reciprocal space as a function of the applied external electric field.

TMDCs can suffer a transition from semiconductor to metal when the applied field is strong enough^{40–42}. However, up to the date the effect of the electric field and the possible modulation of the band gap in small angle twisted TMDCs has not been studied. Since all of these materials could be integrated into new electronic devices where a gate is applied, the study of this effect is of much interest. In this part, we investigate the band gap tuning in twisted bilayer TMDCs by an external electric field applied perpendicularly to the layers, in particular, the twisted bilayer MoS₂ with $\theta = 3.5^\circ$.

Fig. 7 shows the band structure of twisted bilayer MoS₂ with $\theta = 3.5^\circ$ with four different strengths of an

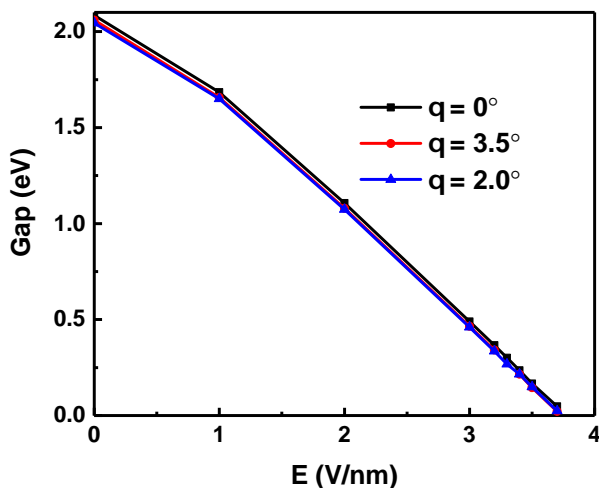


FIG. 8: The band gap of twisted bilayer MoS₂ with different rotation angle as a function of the applied external electric field.

external electric field perpendicular to the layers. The band gap is driven continuously to zero with electric field E and the system changes from semiconductor to metal when E is large enough. This can easily be understood thanks to the so-called giant Stark effect (GSE)⁴³ which, due to the redistribution of the charge density on different layers due to the electric field, splits the bands close to the Fermi level which results in the reduction of the energy gap. This same effect is found in 2H stacking bilayer TMDCs^{40,41} and large angle twisted bilayer WS₂⁴². The evolution of the band gap as a function of E for twisted bilayer MoS₂ with three different rotation angles is plotted in Fig. 8. It is interesting to see that the twist angle does not affect much to the threshold value

where the system becomes metallic. Moreover, it is not only this transition, but also the value of the gap that seems to not be affected by the angle if it is sufficiently small.

5. CONCLUSION

In this paper we have studied the electronic properties of twisted bilayer MoS₂ and their possible tunability by means of an accurate TBPM. We have seen that the flat-band appears when reaching angles sufficiently small. Interestingly, we can tune the value of the gap up to a 5% just by changing the rotation angle. Furthermore, the gap is modulated at different high-symmetry positions of the structure due to the different interlayer couplings that appear. We have also shown that another effective method to tune the band gap is by applying a perpendicular electric field. In fact, the band gap diminishes with increasing electric field and the system can undergo a transition from semiconductor to metal when the field is high enough.

Acknowledgement

This work was supported by the National Science Foundation of China under Grant No. 11774269. F. G. acknowledges support by funding from the European Commission, under the Graphene Flagship, Core 3, grant number 881603, and by the grants NMAT2D (Comunidad de Madrid, Spain), SprQuMat and SEV-2016-0686, (Ministerio de Ciencia e Innovación, Spain). Numerical calculations presented in this paper have been performed on the supercomputing system in the Supercomputing Center of Wuhan University.

* Electronic address: zhen.zhan@whu.edu.cn

† Electronic address: s.yuan@whu.edu.cn

¹ K. S. Novoselov, A. K. Geim, S. V. Morozov, D. Jiang, Y. Zhang, S. V. Dubonos, I. V. Grigorieva, and A. A. Firsov, *Science* **306**, 666 (2004).

² Y. Cao, V. Fatemi, A. Demir, S. Fang, S. L. Tomarken, J. Y. Luo, J. D. Sanchez-Yamagishi, K. Watanabe, T. Taniguchi, E. Kaxiras, et al., *Nature* **556**, 80 (2018).

³ R. Bistritzer and A. H. MacDonald, *Proceedings of the National Academy of Sciences* **108**, 12233 (2011).

⁴ G. Trambly de Laissardi re, D. Mayou, and L. Magaud, *Nano letters* **10**, 804 (2010).

⁵ G. T. De Laissardi re, D. Mayou, and L. Magaud, *Physical Review B* **86**, 125413 (2012).

⁶ K. Kim, A. DaSilva, S. Huang, B. Fallahazad, S. Larentis, T. Taniguchi, K. Watanabe, B. J. LeRoy, A. H. MacDonald, and E. Tutuc, *Proceedings of the National Academy of Sciences* **114**, 3364 (2017).

⁷ Y. Cao, V. Fatemi, S. Fang, K. Watanabe, T. Taniguchi, E. Kaxiras, and P. Jarillo-Herrero, *Nature* **556**, 43 (2018).

⁸ M. Yankowitz, S. Chen, H. Polshyn, Y. Zhang, K. Watanabe, T. Taniguchi, D. Graf, A. F. Young, and C. R. Dean, *Science* **363**, 1059 (2019).

⁹ G. Chen, L. Jiang, S. Wu, B. Lyu, H. Li, B. L. Chittari, K. Watanabe, T. Taniguchi, Z. Shi, J. Jung, et al., *Nature Physics* **15**, 237 (2019).

¹⁰ H. Yoo, R. Engelke, S. Carr, S. Fang, K. Zhang, P. Cazeaux, S. H. Sung, R. Hovden, A. W. Tsen, T. Taniguchi, et al., *Nature Materials* **18**, 448 (2019).

¹¹ A. Kerelsky, L. J. McGilly, D. M. Kennes, L. Xian, M. Yankowitz, S. Chen, K. Watanabe, T. Taniguchi, J. Hone, C. Dean, et al., *Nature* **572**, 95 (2019).

¹² Y. Xie, B. Lian, B. J ck, X. Liu, C.-L. Chiu, K. Watanabe, T. Taniguchi, B. A. Bernevig, and A. Yazdani, *Nature* **572**, 101 (2019).

¹³ Y. Jiang, X. Lai, K. Watanabe, T. Taniguchi, K. Haule, J. Mao, and E. Y. Andrei, *Nature* pp. doi.org/10.1038/s41586-019-1460-4 (2019).

¹⁴ F. Guinea, M. Katsnelson, and A. Geim, *Nature Physics* **6**, 30 (2010).

- ¹⁵ W. Yan, W.-Y. He, Z.-D. Chu, M. Liu, L. Meng, R.-F. Dou, Y. Zhang, Z. Liu, J.-C. Nie, and L. He, *Nature communications* **4**, 1 (2013).
- ¹⁶ H. Shi, Z. Zhan, Z. Qi, K. Huang, E. van Veen, J. Á. Silva-Guillén, R. Zhang, P. Li, K. Xie, H. Ji, et al., *Nature Communications* **11**, 1 (2020).
- ¹⁷ R. Roldán, L. Chirolli, E. Prada, J. A. Silva-Guillén, P. San-Jose, and F. Guinea, *Chemical Society Reviews* **46**, 4387 (2017).
- ¹⁸ B. Amorim, A. Cortijo, F. de Juan, A. Grushin, F. Guinea, A. Gutierrez-Rubio, H. Ochoa, V. Parente, R. Roldán, P. San-Jose, et al., *Physics Reports* **617**, 1 (2016).
- ¹⁹ M. H. Naik and M. Jain, *Physical Review Letters* **121**, 266401 (2018).
- ²⁰ Z. Zhang, Y. Wang, K. Watanabe, T. Taniguchi, K. Ueno, E. Tutuc, and B. J. LeRoy, *arXiv* (2019), 1910.13068.
- ²¹ C. Zhang, C.-P. Chuu, X. Ren, M.-Y. Li, L.-J. Li, C. Jin, M.-Y. Chou, and C.-K. Shih, *Science advances* **3**, e1601459 (2017).
- ²² G. T. De Laissardière, D. Mayou, and L. Magaud, *Physical Review B* **86**, 125413 (2012).
- ²³ R. Roldán, J. A. Silva-Guillén, M. P. López-Sancho, F. Guinea, E. Cappelluti, and P. Ordejón, *Annalen der Physik* **526**, 347 (2014).
- ²⁴ M. H. Naik, S. Kundu, I. Maity, and M. Jain, *arXiv preprint arXiv:1908.10399* (2019).
- ²⁵ S. Yuan, H. De Raedt, and M. I. Katsnelson, *Physical Review B* **82**, 115448 (2010).
- ²⁶ G. Yu, Z. Wu, Z. Zhan, M. I. Katsnelson, and S. Yuan, *NPJ Computational Materials* **5**, 1 (2019).
- ²⁷ S. Fang, R. K. Deho, S. N. Shirodkar, S. Lieu, G. A. Tritsarolis, and E. Kaxiras, *Physical Review B* **92**, 205108 (2015).
- ²⁸ E. Cappelluti, R. Roldán, J. Silva-Guillén, P. Ordejón, and F. Guinea, *Physical Review B* **88**, 075409 (2013).
- ²⁹ J. Silva-Guillén, P. San-Jose, and R. Roldán, *Applied Sciences* **6**, 284 (2016).
- ³⁰ R. Roldán, M. P. López-Sancho, F. Guinea, E. Cappelluti, J. Á. Silva-Guillén, and P. Ordejón, *2D Materials* **1**, 034003 (2014).
- ³¹ S. Huang, X. Ling, L. Liang, J. Kong, H. Terrones, V. Meunier, and M. S. Dresselhaus, *Nano letters* **14**, 5500 (2014).
- ³² A. A. Puretzky, L. Liang, X. Li, K. Xiao, B. G. Sumpter, V. Meunier, and D. B. Geohegan, *ACS nano* **10**, 2736 (2016).
- ³³ A. M. van Der Zande, J. Kunstmann, A. Chernikov, D. A. Chenet, Y. You, X. Zhang, P. Y. Huang, T. C. Berkelbach, L. Wang, F. Zhang, et al., *Nano letters* **14**, 3869 (2014).
- ³⁴ K. Liu, L. Zhang, T. Cao, C. Jin, D. Qiu, Q. Zhou, A. Zettl, P. Yang, S. G. Louie, and F. Wang, *Nature communications* **5**, 4966 (2014).
- ³⁵ P.-C. Yeh, W. Jin, N. Zaki, J. Kunstmann, D. Chenet, G. Arefe, J. T. Sadowski, J. I. Dadap, P. Sutter, J. Hone, et al., *Nano letters* **16**, 953 (2016).
- ³⁶ S. Carr, D. Massatt, S. Fang, P. Cazeaux, M. Luskin, and E. Kaxiras, *Physical Review B* **95**, 075420 (2017).
- ³⁷ Z. Zhan, Y. Zhang, Y. Guodong, F. Guinea, J. Á. Silva-Guillén, and Y. Shengjun, *Unpublished* (2020).
- ³⁸ Y. Zhang, T.-T. Tang, C. Girit, Z. Hao, M. C. Martin, A. Zettl, M. F. Crommie, Y. R. Shen, and F. Wang, *Nature* **459**, 820 (2009).
- ³⁹ K. F. Mak, C. H. Lui, J. Shan, and T. F. Heinz, *Physical review letters* **102**, 256405 (2009).
- ⁴⁰ A. Ramasubramaniam, D. Naveh, and E. Towe, *Physical Review B* **84**, 205325 (2011).
- ⁴¹ Q. Liu, L. Li, Y. Li, Z. Gao, Z. Chen, and J. Lu, *The Journal of Physical Chemistry C* **116**, 21556 (2012).
- ⁴² Z. Zhang, J. Li, G. Yang, and G. Ouyang, *The Journal of Physical Chemistry C* **123**, 19812 (2019).
- ⁴³ K. H. Khoo, M. S. Mazzoni, and S. G. Louie, *Physical Review B* **69**, 1 (2004).